AIP | The Journal of Chemical Physics

Morphological and chemical influences on alumina-supported palladium catalysts active for the gas phase hydrogenation of crotonaldehyde

A. R. McInroy, A. Uhl, T. Lear, T. M. Klapötke, S. Shaikhutdinov, S. Schauermann, G. Rupprechter, H.-J. Freund, and D. Lennon

Citation: The Journal of Chemical Physics **134**, 214704 (2011); doi: 10.1063/1.3593472
View online: http://dx.doi.org/10.1063/1.3593472
View Table of Contents: http://scitation.aip.org/content/aip/journal/jcp/134/21?ver=pdfcov
Published by the AIP Publishing

Morphological and chemical influences on alumina-supported palladium catalysts active for the gas phase hydrogenation of crotonaldehyde

A. R. McInroy,[1] A. Uhl,[1,2] T. Lear,[1] T. M. Klapötke,[3] S. Shaikhutdinov,[2] S. Schauermann,[2] G. Rupprechter,[4] H.-J. Freund,[2] and D. Lennon[1,a)]
[1]*Department of Chemistry, Joseph Black Building, University of Glasgow, Glasgow G12 8QQ, Scotland, UK*
[2]*Fritz-Haber-Institut der Max-Planck-Gesellschaft, Chemical Physics Department, Faradayweg 4-6, D-14195 Berlin, Germany*
[3]*Department of Chemistry, Ludwig-Maximilian University of Munich, Butenandtstr. 5-13 (Haus D), D-81377 Munich, Germany*
[4]*Institute of Materials Chemistry, Vienna University of Technology, Veterinärplatz 1, Bau GA, 4. Stock, 1210 Wien, Austria*

(Received 5 November 2010; accepted 2 May 2011; published online 7 June 2011)

A series of five alumina-supported palladium catalysts have previously been prepared and characterised by a combination of CO chemisorption and infrared spectroscopy. The reactive attributes of these catalysts are examined using the hydrogenation of crotonaldehyde as a test reaction, using a modified infrared gas cell as a batch reactor. Periodic scanning of the infrared spectrum of the gaseous phase present over the Pd/Al_2O_3 catalysts was used to construct reaction profiles. Four of the catalysts were able to facilitate a 2-stage hydrogenation process (crotonaldehyde → butanal → butanol), whilst one catalyst was totally selective for the first stage hydrogenation process (crotonaldehyde → butanal). Rate coefficients for the first and second stage hydrogenation processes are normalised to the number of surface palladium atoms for the particular catalyst. Correlation of these kinetic parameters as a function of mean particle size indicates the first stage process to be *structure insensitive*, whilst the second stage hydrogenation is *structure sensitive*. Chlorine residues associated with the preparative process of one of the catalysts is seen to selectively poison the second stage hydrogenation process for that catalyst. Structure/activity relationships are considered to explain the observed trends. © *2011 American Institute of Physics*. [doi:10.1063/1.3593472]

I. INTRODUCTION

Modern heterogeneous catalysis seeks to make catalysts that convey high selectivity for specified reactions. Whereas in the past catalyst manufacturers have tended to favour an empirical approach to catalyst optimisation that is backed up by an appreciation of a reaction mechanism,[1] it is increasingly being realised that the development of *structure/activity relationships* can be used to "design" catalysts that are capable of delivering high yields of product over extended periods of time.[2–4] Adopting this concept, this communication seeks to develop a link between catalyst manufacturing procedures, a catalyst characterisation strategy and the control of branching within a step-wise reaction sequence of modest complexity. Specifically, the task is to use the hydrogenation of crotonaldehyde in the gas phase to determine the reaction characteristics of five alumina-supported palladium catalysts, the morphologies of which have previously been investigated by a combination of CO chemisorption and infrared spectroscopy.[5] Thence, via an analysis of the reaction profiles and associated rate coefficients, a structure/activity relationship will be considered, which can be correlated with options available in the original catalyst manufacturing process.

Supported palladium catalysts are used widely in heterogeneous catalysis, with alumina-supported palladium finding wide application, not least in selective hydrogenation reactions.[6,7] In an attempt to better understand how different preparative routes can influence the distribution of active sites present on finely divided palladium crystallites, a previous study used infrared spectroscopy of chemisorbed CO to determine morphological traits of a range of Pd/Al_2O_3 catalysts.[5] That work followed on from an analysis of a "model" high surface area alumina-supported palladium catalyst.[8] In addition to identifying the dominant Pd facets encountered on using a variety of precursor compounds, the work additionally highlighted the potential of halide salts to self-poison particular sites. Preliminary studies using propene hydrogenation as a test reaction suggested that a relatively reduced activity seen for a Pd/Al_2O_3 catalyst prepared from $PdCl_2$ occurred as a consequence of residual chlorine decorating edge sites.[5] Elemental analysis revealed a residual chlorine content of 5.4 wt. %, with the chlorine presence being associated with aspects of the preparative process for this particular catalyst.[5] Against this background it was deemed informative to compare these five catalysts in a more discerning test reaction. Crotonaldehyde hydrogenation was selected for that task.

Crotonaldehyde ($CH_3CH = CHCHO$) is an example of an α,β-unsaturated aldehyde. A reaction scheme for the hydrogenation pathways is shown in Fig. 1, with butanal (buytyraldehyde) and 2-butene-1-ol (crotyl alcohol) being

a)Author to whom correspondence should be addressed. Electronic mail: d.lennon@chem.gla.ac.uk. Telephone: (+44)-(0)-141-330-4372. Fax: (+44)-(0)-141-330-4888.

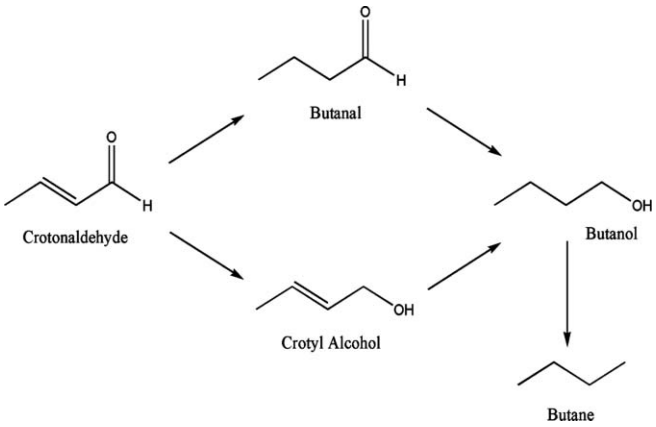

FIG. 1. Reaction scheme for the hydrogenation of crotonaldehyde. Stage 1 hydrogenation involves the hydrogenation of crotonaldehyde to form butanal. Stage 2 hydrogenation involves the hydrogenation of butanal to form butanol.

primary products formed from the initial hydrogenation process.[9] Both of these materials can then be further hydrogenated to produce butanol. Most work concentrates on optimising the formation of crotyl alcohol, which as an unsaturated alcohol represents an important intermediate in the field of fine chemicals synthesis.[10,11]

Crotonaldehyde hydrogenation has been studied using a wide range of supported metal catalysts.[10] For example, Englisch *et al.* looked at silica and titania-supported platinum catalysts[9] and demonstrated the reaction to be *structure sensitive*[12(a),13(a),(b)] over these materials. For Pt/SiO_2, the selectivity to crotyl alcohol increases with increasing particle size as a consequence of the larger particles emphasizing (111) facets, which favour crotonaldehyde adsorption via the carbonyl bond.[9] Subsequent work by Gebauer-Henke *et al.* looking at platinum catalysts supported on gallium oxide showed the use of this support material increased the C = O bond hydrogenation selectivity (i.e., selectivity to crotyl alcohol) whilst maintaining high activity.[14] Following on from the initial studies by Bailie and Hutchings,[15] Zanella *et al.* have shown that gold catalysts are active for crotonaldehyde hydrogenation and exhibit a higher selectivity to crotyl alcohol than butanal. Additionally, the reaction is shown to be strongly structure sensitive, as illustrated by an increase in activity and turn over frequency for gold particles of ~2 nm.[16] Claus and Hofmeister have examined silver catalysts and report trends more aligned to those seen for Pt catalysts,[9] namely high selectivity to crotyl alcohol was obtained on catalysts containing mainly silver particles with Ag(111) surface planes.[11] More recently Ramos-Fernández *et al*. have looked at Pt/Ta_2O_5-ZrO_2 catalysts and considered the effect of support composition, with their studies indicating a probable role for a metal-support interaction with these catalysts.[17]

There has been much less interest in looking at the hydrogenation of α,β-unsaturated aldehydes over Pd on non-reducible supports, as these catalysts tend not to produce unsaturated alcohols as the main product in gas phase hydrogenations.[11] Divakar *et al.* compared a palladium intercalated vermiculite catalyst against a commercial Pd/C catalyst with both catalysts showing favourable selectivity to the unsaturated alcohol (crotyl alcohol) at a reaction temperature of 200 °C.[18] Whilst concentrating on a palladium doped acidic resin, functioning as a bifunctional catalyst and operating within a supercritical carbon dioxide ($scCO_2$) medium, Seki *et al.* have used 1% Pd/Al_2O_3 and Pd/C catalysts to hydrogenate crotonaldehye.[19] Within the $scCO_2$ environment both Pd/Al_2O_3 and Pd/C exhibit high conversions but the respective selectivities for butanal are 70% and 55%, whereas the selectivity for butanol is 9% for both catalysts. In this manner, these trends are generally consistent with the expectation enunciated by Rylander that supported palladium catalysts will yield butanal rather than crotyl alcohol and that the reaction will stop at the first stage of the hydrogenation process, with no formation of butanol.[20(a),(b)]

In addition to studies on high surface area catalysts, crotonaldehyde adsorption and hydrogenation have been studied on metal single crystals using the tools of surface science. Jesús and Zaera used reflection absorption infrared spectroscopy and temperature programmed desorption (TPD) to study the adsorption of crotonaldehyde on Pt(111) and identified a strong di σ(C-C) interaction with the surface.[21] Janin *et al.* have examined Pt(111) and Pt/Sn alloys and report an interaction to the surface through the C = C bond and the aldehydic oxygen.[22] Jerdev *et al.* have examined the hydrogenation of crotonaldehyde over Sn/Pt(111) alloy model catalysts and, in contrast to results for supported Pt catalysts,[9] butanal was formed as the main product.[23] Haubrich *et al.* have used a combination of vibrational electron energy loss spectroscopy, TPD and low energy electron diffraction to characterise crotonaldehyde adsorption on Pt(111) and Pt-Sn alloys and demonstrate the complexity of adsorption geometries possible with this adsorption system.[24] Following up on earlier work on Pt(111),[25] Lambert and co-workers have used x-ray photoelectron spectroscopy and near edge X-ray adsorption fine structure spectroscopy to understand how the presence of sulphur on a Cu(111) single crystal can activate the surface towards crotyl alcohol formation.[26] That work nicely connects with preceding studies by Hutchings and co-workers examining supported copper catalysts.[27,28] Somorjai's group have recently considered aspects of crotonaldehyde hydrogenation on Pt nanaoparticles. First, Somorjai and Park have shown that increasing the particle size of Pt nanoparticles decreases the butanal production whilst crotyl alcohol production increases.[2] These trends are in good agreement with Englisch *et al.*[9] Subsequent work from Somorjai's group has then used sum-frequency generation to follow the hydrogenation of crotonaldehyde over Pt(111) and Pt(100) single crystals, with both surfaces exhibiting little *structure sensitivity*.[29]

Accepting that palladium catalysts have no role in producing the unsaturated alcohol from the hydrogenation of crotonaldehyde, this work is interested in linking first stage (crotonaldehyde → butanal) and second stage (butanal → butanol) hydrogenation activity with the structure of the palladium crystallites. Specifically, the work seeks to explore structure/activity relationships for alumina-supported palladium catalysts applied to the crotonaldehyde hydrogenation reaction. Reaction testing is undertaken using infrared spectroscopy, where an infrared cell is used as a batch reactor. Periodic scanning of the gas phase enables the change in

the gaseous phase present over the catalyst to be determined as a function of time.[30–32] Whereas the preferred analytical approach for monitoring catalytic reactions utilises plug-flow micro-reactors coupled to in-line chromatographic techniques (e.g., gas liquid chromatography) or mass spectrometry, the *in situ* infrared method offers the advantage that, providing the reacting components can be satisfactorily identified within a mixture of gases, then the rapidly acquired spectrum provides information on gases that are in direct exchange with the catalyst surface. The benefits and disadvantages of this use of infrared spectroscopy are considered elsewhere.[32] Further, an additional benefit not considered in the earlier studies[30–32] is that the resulting infrared spectra potentially contain information on conformational options attainable for the reagents and products throughout the full reaction coordinate. Although such considerations do not feature in this work, it is possible that conformational branching could be linked to selectivity pathways. A subsequent paper will consider these options in relation to the hydrogenation of 1,3-pentadiene.[33] Such precise molecular detail would not be readily accessible via conventional micro-reactor/in-line chromatographic analysis.

There is no doubt that Pd is effective at reducing the C = C moiety but this work seeks to establish whether particular crystallites of palladium can influence hydrogenation of the C = O group. The sequential nature of the crotonaldehyde hydrogenation sequence over this metal (crotonaldehyde → butanal → butanol) presents an effective way of assessing how metal dispersion and particle shape can influence the inter-conversion from an aliphatic aldehyde to a primary alcohol as part of a series of stepwise reactions. After all, an awareness of how reaction pathways are linked (or not) to metal crystallite morphology is an important requirement in being able to design highly selective catalysts.

II. EXPERIMENTAL

A. Catalyst preparation and characterisation

Five alumina-supported Pd catalysts were investigated. Two were prepared using palladium(II) nitrate as a precursor, one each using Pd(II) chloride and palladium(II) acetylacetonate, and finally, one was prepared via the decomposition of the unstable precursor tetraammine palladium(II)tetraazidopalladate(II). These samples are identified by the following terms: 1 wt. % $Pd(NO_3)_2$, 5 wt. % $Pd(NO_3)_2$, 1 wt. % $PdCl_2$, 1 wt. % Pd(acac) and 10 wt. % Pd(azide). Details of their preparative procedures and their characterisation, including deductions on palladium crystallite morphology, are presented elsewhere.[5] The interaction of the 1 wt. % $Pd(NO_3)_2$ and 5 wt. % $Pd(NO_3)_2$ catalysts with CO have been further examined by a combination of adsorption isotherm measurements, temperature programmed desorption, and temperature programmed oxidation studies.[34]

B. Reaction testing

The reactor was based around a modified Graseby-Specac 5660 heated gas cell fitted with KBr windows and a 20140 automatic temperature controller. An injection septum within the cell enabled reagents to be added to the reaction system. The tubular cell had no facility for further mixing or re-circulation of gases. Two Brooks 5850E mass flow devices controlled the flow of hydrogen (BOC, 99.995% purity) and helium (BOC, CP grade 99.999% purity) via an in-line purifier (Messer Grieshiem Oxisorb) into a 50 cm^3 stainless steel mixing vessel that was packed with glass beads before entering into the reaction cell. A back-pressure regulator plus pressure gauge (Norgen) and shut-off valves allowed the cell to be isolated and the pressure monitored. The reactor was housed within a Nicolet Avatar 360 FTIR spectrometer equipped with a deuterated triglycine sulphate detector. The reactor is connected to the spectrometer internal gas purge facility via rubber sleeves. The spectrometer is continually purged with dry air, from which the CO_2 component has been removed (Donaldson Ultrafilter). These arrangements minimise atmospheric contributions to the infrared spectrum.

The catalyst was loaded into the reactor as a pressed disc. For all the studies presented in this study the catalyst was mounted within a glass sample holder that locates within the base of the cell, so that the catalyst was not in the path of the infrared beam. In this way, all spectra presented arise from the composition of the gaseous phase, with no contribution from the catalyst or the catalyst surface. This simplifies the analysis considerably. Subsequent studies could involve the catalyst being mounted vertically, so that the infrared beam directly samples the catalyst as well as the reacting gas. However, those experiments were not performed on this occasion. The use of a pressed disc ensures that the sample remains in position throughout the course of the experiment and that no "fines" are inadvertently removed from the cell during the various gas switching operations. The rate of crotonaldehyde hydrogenation was directly proportional to the mass of catalyst used, consistent with the reaction being under kinetic control with no mass transport restrictions. Further work would be required to explore this matter further.

The catalyst mass, quantity of hydrocarbon, and pressure of hydrogen were selected to yield a full hydrogenation profile in a time that was sufficiently long so that infrared spectra of sufficient signal/noise ratio could be repeatedly recorded during that interval, in order to define a representative reaction profile. In this manner, ~20 mg of the catalyst was pressed into a thin disc using a 13 mm die (Specac) pressurised at 12 tonnes by a hydraulic press (Perkin Elmer). The catalyst disc was reduced in the following manner: The cell temperature was maintained at 303 K and a mixture of 10% H_2 / 90% He was passed through the reactor at a flow rate of 20 ml min^{-1} for 30 min. The hydrogen composition was increased to yield an equimolar mixture of hydrogen and helium at the same flow rate and the temperature was increased to 423 K, and then maintained at that temperature. After 30 min under these conditions, the reactor was isolated at a pressure of 900 torr (0.12 MPa). A liquid chromatography syringe (Hamilton Bonaduz) was used to inject a 5.0 μl aliquot of crotonaldehyde into the cell via the septum. Crotonaldehyde (Aldich, 99 + %) was used without further purification. Scanning of the infrared spectrum commenced as soon as the injection of the unsaturated aldehyde was complete. This combination of reagents results in a hydrogen:hydrocarbon ratio of 47:1 and a hydrocarbon:Pd(s) ratio of 77:1 for the $PdCl_2$

catalyst, i.e., hydrogen is in excess of the hydrocarbon and the hydrocarbon is in excess of palladium surface atoms. Thus, the infrared cell is acting as a batch reactor under conditions where reasonable conversions represent multiple turnovers, unhindered by the availability of hydrogen. Infrared spectra were recorded at a resolution of 4 cm^{-1}, co-adding eight scans and requiring an acquisition time of ~10 s. The reaction temperature was maintained at 423 K for all the reactions studied and ensured that all the reagents remained in the gaseous phase. All measurements were performed at least in duplicate, with representative datasets being presented here. It is acknowledged that due to different characteristics of the reactors, the activation procedure differs slightly from that used in the CO chemisorption measurements.[5] It is anticipated that any consequential deviations in Pd structure will be minimal.

Hydrogenation experiments on an alumina disc (no Pd) that had been treated in the same manner as outlined above showed no conversion of crotonaldehyde. Given the relative simplicity of the experimental arrangement, the reacting gases obey the Beer-Lambert law, thereby permitting calibration curves to be readily produced. In this way, the number of moles of the majority of reagents could be reliably determined from the integrated infrared intensity for a particular vibrational feature. Butanal (Aldrich, 99.5%) and 1-butanol (Aldrich, 99.8%) were used as calibrants. Butanal hydrogenation experiments were also performed and were undertaken in exactly the same way as for the crotonaldehyde experiments.

C. Butanal adsorption measurements

Infrared adsorption experiments were performed using a Nicolet Nexus FTIR spectrometer fitted with a MCT high D* detector. Measurements were performed in diffuse reflectance mode using a SpectraTech Smart diffuse reflectance cell and environmental chamber. The cell was connected to a vacuum manifold/gas flow apparatus that provides control of the flow of gases into the infrared cell. This includes an in-line sample loop for sequential dosing of the catalyst in a pulse-flow arrangement. A constant stream of high purity helium (BOC CP grade, 99.999%) fitted with an in-line purifier (Messer Grieshiem Oxisorb) was passed over the catalyst at all times (30 ml min^{-1}, 1.5 atm). The samples were activated *in situ* using the procedure outlined elsewhere.[5] Background spectra were recorded post-activation at 293 K. Butanal (Aldrich, 99.5%) was dosed on to the catalyst at 293 K using pulse-flow techniques.[35] Ancillary experiments confirmed that a 20 min delay after each dosing pulse was sufficient time for the adsorbate to be completely removed from the environmental chamber. After dosing, the spectrum was recorded (512 scans, resolution 4 cm^{-1}). The diffuse reflectance spectra are presented as background subtractions, where a spectrum of the activated catalyst has been subtracted from the dosed spectrum. No baseline or offset corrections were made.

III. RESULTS AND DISCUSSION

In order to illustrate the trends observed for all of the five catalysts under consideration here, two catalysts are deemed to be representative: the 1% $PdCl_2$ and the 5% $Pd(NO_3)_2$. The reaction characteristics for both of these samples are presented below.

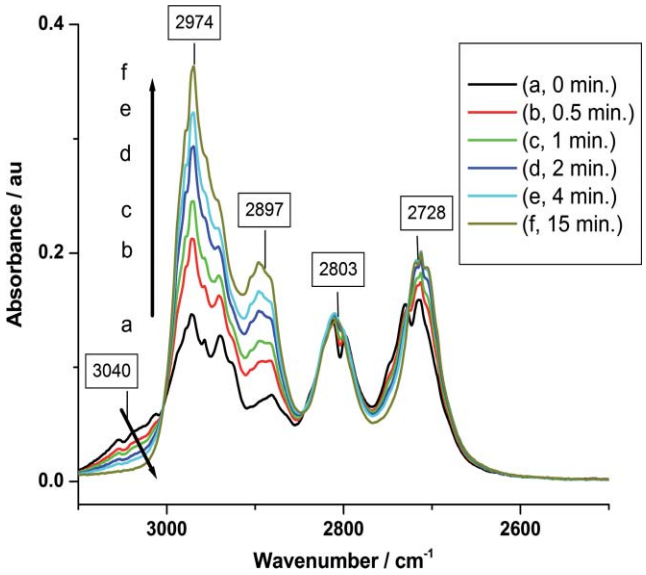

FIG. 2. Infrared spectrum (3100–2500 cm^{-1}) as a function of time for the hydrogenation of crotonaldehyde over the 1% $PdCl_2$ catalyst: (a) 0, (b) 0.5, (c) 1, (d) 2, (e) 4, and (f) 15 min. The solid arrows indicate intensity trends for bands at 3040 and 2974 cm^{-1}.

A. 1 wt. % $PdCl_2/Al_2O_3$

The catalyst was reduced; the cell charged with hydrogen then crotonaldehyde injected in to the cell and the infrared spectrum of the gaseous phase periodically scanned. Figure 2 shows the infrared spectrum about the C-H stretching region over a period of 15 min. At short times intensity is seen about 3040 cm^{-1}, which corresponds to olefinic C-H stretching features. Band heads at 2974 and 2897 cm^{-1} are due to aliphatic C-H stretching modes. The bands at 2803 and 2728 cm^{-1} are assigned to aldehyde C-H bands, with the doublet being due to respectively a Fermi resonance effect between the aldehyde C-H stretching vibration and the first overtone of the in-plane C-H bending vibration (C-H rock).[36(a)]

On increasing time the intensity of the olefinic C-H stretching region diminishes, whilst the intensity in the aliphatic region (2980 and 2900 cm^{-1}) increases. This indicates the occurrence of the first stage hydrogenation process, where crotonaldehyde is being progressively hydrogenated to form butanal. Throughout this period the intensity of the aldehyde C-H bands at 2803 and 2728 cm^{-1} are effectively unchanged. The consistency of these two modes confirms that the aldehyde unit is intact and remains resistant to hydrogenation on this catalyst.

Figure 3 presents the corresponding spectra for the C = O stretching region. At short times, two sharp features at 1720 and 1710 cm^{-1}, corresponding to ν(C = O) of crotonaldehye are clearly visible. On increasing time these features collapse whilst there is a concomitant increase in a broad band centred at 1751 cm^{-1}. In fact the high wavenumber feature is also due to a ν(C = O) mode but now it represents a

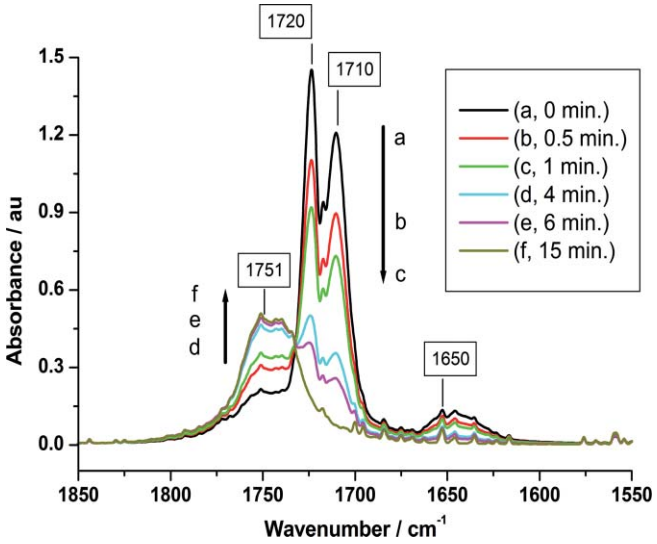

FIG. 3. Infrared spectrum (1850–1550 cm^{-1}) as a function of time for the hydrogenation of crotonaldehyde over the 1% $PdCl_2$ catalyst: (a) 0, (b) 0.5, (c) 1 (d) 4, (e) 6, and (f) 15 min. Arrows indicate the direction of band intensity as a function of reaction time. The symbols (a)–(c) are aligned with band intensity at 1710 cm^{-1}, whereas symbols (d)–(f) are aligned with band intensity at 1750 cm^{-1}.

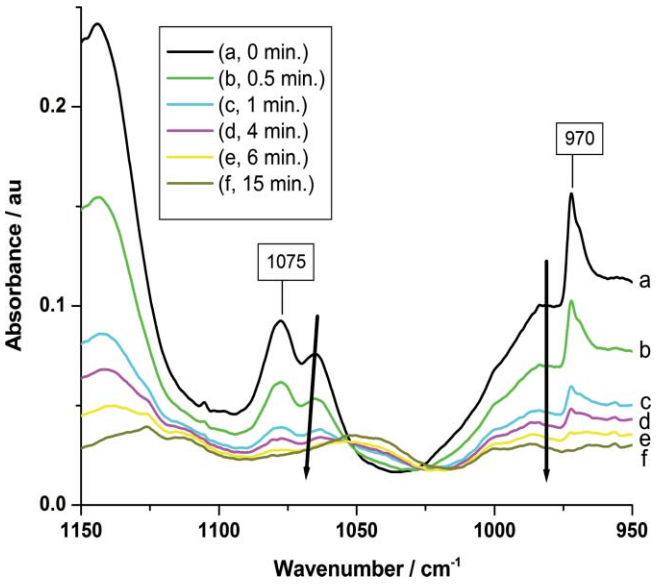

FIG. 4. Infrared spectrum (1150–950 cm^{-1}) as a function of time for the hydrogenation of crotonaldehyde over the 1% $PdCl_2$ catalyst: (a) 0, (b) 0.5, (c) 1 (d) 4, (e) 6, and (f) 15 min. The solid arrows indicate intensity trends for bands at 1075 and 970 cm^{-1}.

saturated aldehyde rather than the original unsaturated form. In crotonaldehyde the carbonyl group is in conjugation with the double bond. Once that double bond is hydrogenated, the conjugation is lost and the isolated $\nu(C = O)$ shifts to high wavenumber.[36(a)(b),37(a)] The isosbestic point at 1730 cm^{-1} is entirely consistent with the simple inter-conversion of crotonaldehyde to butanal. At short reaction times a broad band about 1650 cm^{-1} is present which is attributed to the $\nu(C = C)$ of crotonaldehyde. This reduces in intensity in a similar fashion to that seen for the 1720 and 1710 cm^{-1} peaks. These profiles are consistent with the trends observed in Fig. 2, where only first stage hydrogenation (crotonaldehyde → butanal) is seen. If crotyl alcohol was formed during the first stage process, then there would be residual intensity due to $\nu(C = C)$. However, as Fig. 3 shows the loss of this band to exactly follow the decrease in the 1720 and 1710 cm^{-1} doublet, then it is deduced that no crotyl alcohol is being formed during the crotonaldehyde conversion process.

Claus has previously described a mechanism that accounts for the hydrogenation of crotonaldehyde over a range of metals.[10] That work identifies a role for π-allylic and oxygen-π-allylic intermediates that can lead on to products such as allylcarbinol, 2-butanol, ethyl methyl ketone, etc. None of these products are identified in the gas phase spectra seen here indicating that over $PdCl_2$ a 3,4 H-addition process (leading to butanal formation) dominates the crotonaldehyde conversion process.

Figure 4 presents the infrared spectrum in the 1150–950 cm^{-1} region. Two sets of bands at 1075 and 970 cm^{-1} are seen to decrease in intensity as a function of time. The doublet about 1075 cm^{-1} is assigned to an in-plane CH_3 rock, whilst the 970 cm^{-1} feature is assigned to a CH = CH out of plane antisymmetric deformation of crotonaldehyde.[38] The reduction in intensity of both of these features over the 15 min period replicates the trends seen for the unsaturated modes in Figs. 2 and 3 and provides further evidence for the reduction of the C = C bond in crotonaldehyde. Moreover, the absence of any development of a band in the 1075–1000 cm^{-1} region, indicative of an out of phase C-C-O stretch,[36(d),37(b)] additionally confirms the absence of crotyl alcohol in the head space.

With reference to calibration curves (not shown), the intensity of the $\nu(C = O)$ band for crotonaldehyde at 1720 cm^{-1} (or the loss of the $\nu(C = C)$ mode at 1649 cm^{-1}) and the $\nu(C = O)$ band for butanal at 1751 cm^{-1} can be used to determine the quantity of each reagent present in the gas phase at any time. Figure 5 presents the resulting reaction profile, which shows a simple conversion from crotonaldehyde to butanal. No other products were detected. Moreover, the curves are well described by simple exponentials (decay and growth), indicating the process to conform to first order reaction kinetics. Consequently, a rate coefficient for this reaction can be readily obtained[39(a)] (see Sec. III B). Continued scanning for 12 times the half-life for this reaction showed only butanal to be present, establishing that this catalyst could not hydrogenate the carbonyl group under these reaction conditions even at long reaction times. These observations are entirely consistent with the views expressed by Rylander, where he reports that palladium based catalysts are highly selective for C = C hydrogenation but ineffective for C = O hydrogenation.[20(a)]

Figure 5 also presents the mass balance for this reaction which is determined from the sum of the absolute values of the reagents/products (only crotonaldehyde and butanal in this case) at time, t. Up to 6 min a small excess of up to +11% is seen, which diminishes to –4% (i.e., 96% of the incident moles) at 15 min. The excess at the beginning is thought to reflect the error in obtaining a mass balance evaluation using the *in situ* spectroscopic approach adopted here, with accurate definition of the areas of isolated vibrational bands thought to

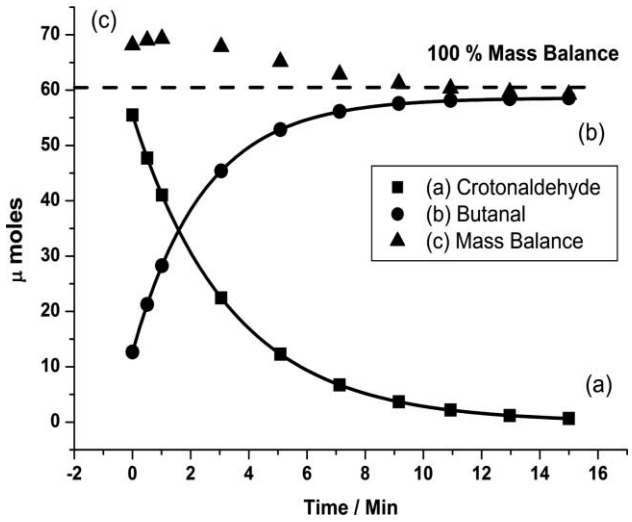

FIG. 5. Reaction profile for the hydrogenation of crotonaldehyde over the 1% $PdCl_2$ catalyst: (a) crotonaldehyde, (b) butanal, and (c) mass balance determined from (a) + (b). The solid lines are interpolations between data points, whilst the dashed line corresponds to 100% mass balance.

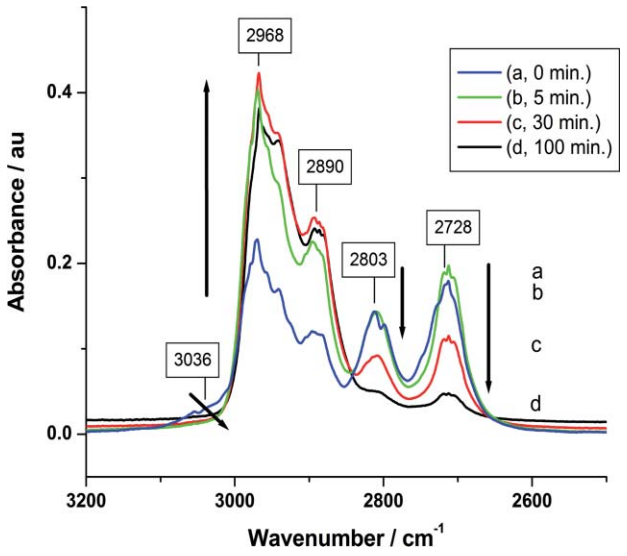

FIG. 6. Infrared spectrum (3200–2500 cm^{-1}) as a function of time for the hydrogenation of crotonaldehyde over the 5% $Pd(NO_3)_2$ catalyst: (a) 0, (b) 5, (c) 30, and (d) 100 min. Arrows indicate the direction of band intensity as a function of reaction time.

be the greatest source of error.[32] Accepting that limitation, Fig. 4 is interpreted as indicating a nearly complete mass balance for this reaction.

As discussed above, the observation that a palladium catalyst will selectively produce butanal is in agreement with Rylander,[20(a)] although he does report one exception to this rule.[20(b),40] Further, Seki *et al.* note some formation of butan-1-ol for their 1% Pd/Al_2O_3 catalyst with the reaction performed in $scCO_2$ reporting selectivities for butanal and butan-1-ol of 70 and 9% respectively.[19] In the case of the 1 wt. % $PdCl_2/Al_2O_3$ catalyst under examination here, the selectivity to butanal is 100%.

B. 5 wt. % $Pd(NO_3)_2/Al_2O_3$

The infrared spectrum in the C-H stretching region of the gaseous phase present above the 5 wt. % $Pd(NO_3)_2/Al_2O_3$ as a function of time is presented in Fig. 6. Here the trends observed for the various features differ significantly from those encountered in Fig. 2. Although the concomitant loss of the olefinic features (bands above 3000 cm^{-1}) with the increase of the aliphatic ν(C-H) features (bands above 2840 cm^{-1}) is comparable to that seen in Fig. 2, noticeable differences are seen with the two features at 2803 cm^{-1} and 2728 cm^{-1}. Here, both the aldehyde C-H bands [ν(C-H) and 2 x ρ (C-H)] decrease on increasing reaction time, whereas they remained roughly constant in Fig. 2. The loss of intensity for both these features indicates that the carbonyl group is being hydrogenated. At 100 min this feature exhibits negligible intensity and the ν(C-H) signature is comprised of a predominantly aliphatic unit. These observations indicate that first stage and second stage hydrogenation is occurring in this case on this catalyst.

The infrared spectra for the diagnostic $\nu(C=O)$ region are presented in Fig. 7. Again contrasting with the 1 wt. % $PdCl_2/Al_2O_3$ catalyst (Fig. 3), two stages are clearly defined. First, the two sharp peaks at 1720 and 1710 cm^{-1} arising from the presence of crotonaldehyde decrease on increasing time, with a related shift to lower wavenumber as seen in Fig. 3. The shift is then followed by an increase in intensity at 1750 cm^{-1}. The isosbestic point at 1730 cm^{-1} is retained during this transition. However, on extended times the isosbestic point is lost and the broad feature about 1750 cm^{-1} is seen to progressively decrease, so that by 100 min this band assigned to the $\nu(C=O)$ of butanal has minimal intensity. Thus, the profile of this highly diagnostic feature can be described by a reduction in intensity of the conjugated carbonyl band, which shifts to higher wavenumber and then increases in intensity up to

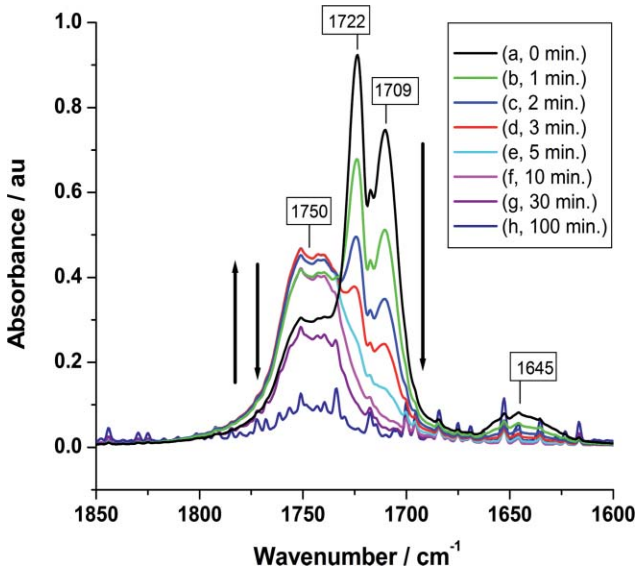

FIG. 7. Infrared spectrum (1850 – 1600 cm^{-1}) as a function of time for the hydrogenation of crotonaldehyde over the 5% $Pd(NO_3)_2$ catalyst: (a) 0, (b) 1, (c) 2 (d) 3, (e) 5, (f) 10 (g) 30, and (h) 100 min. The solid arrows indicate intensity trends for bands at 1750 and 1722 cm^{-1}.

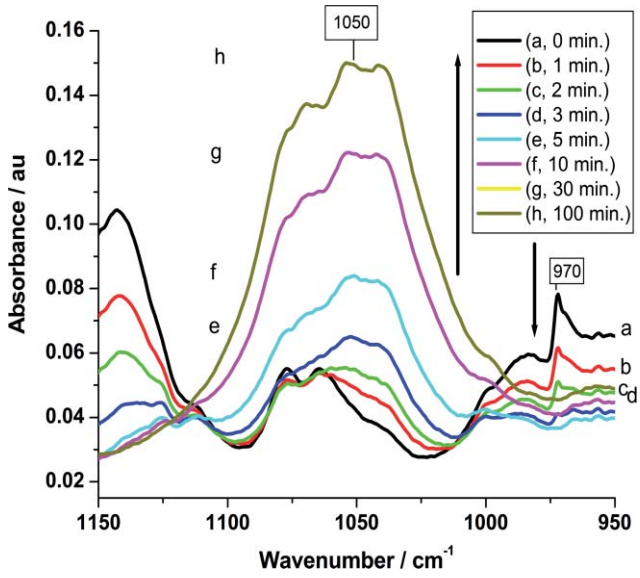

FIG. 8. Infrared spectrum (1150 – 950 cm^{-1}) as a function of time for the hydrogenation of crotonaldehyde over the 5% $Pd(NO_3)_2$ catalyst: (a) 0, (b) 1, (c) 2 (d) 3, (e) 5, (f) 10 (g) 30, and (h) 100 min. The arrows indicate the direction of band intensity at 1050 and 970 cm^{-1} as a function of reaction time. The symbols (a)–(d) are aligned with band intensity at 970 cm^{-1}, whereas symbols (e)–(h) are aligned with band intensity at 1050 cm^{-1}.

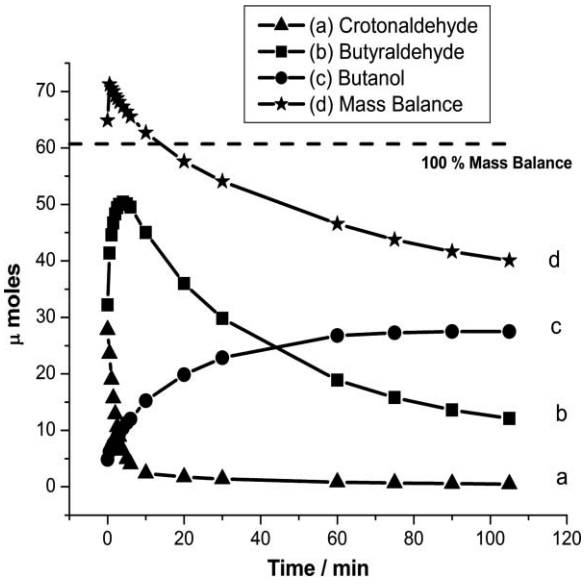

FIG. 9. Reaction profile for the hydrogenation of crotonaldehyde over the 5% $Pd(NO_3)_2$ catalyst: (a) crotonaldehyde, (b) butanal, (c) butanol, and (d) mass balance determined from (a) + (b) + (c). The solid lines are interpolations between data points, whilst the dashed line corresponds to 100% mass balance.

a reaction time of ~3 min. Thereafter this band decreases in intensity on increasing reaction time.

At short reaction times, the broad ν(C = C) band of crotonaldehyde about 1650 cm^{-1} is present, which attenuates in phase with the 1720 and 1710 cm^{-1} ν(C = O) peaks. These profiles are consistent with the trends observed in Fig. 6, where first stage hydrogenation (crotonaldehyde → butanal) is followed by second stage hydrogenation (butanal → butanol). Crotyl alcohol makes no noticeable contribution to the spectra.

Figure 8 presents the infrared spectrum corresponding to the C-O stretching region. At short times the crotonaldehyde in-plane CH_3 rock (1075 cm^{-1}) and the CH = CH out of plane antisymmetric deformation (970 cm^{-1}) are evident. The latter band progressively diminishes on increasing time, consistent with conversion of crotonaldehyde. However, the former becomes swamped by the substantial growth of a series of bands about 1050 cm^{-1} that are assigned to an out of phase C-C-O stretch of a primary alcohol.[36(e),37(b)] The increase in intensity of this feature is clear evidence for the formation of butan-1-ol. A ν(O-H) feature about 3700 cm^{-1} (not shown) follows the trend seen for the 1050 cm^{-1} band. In a similar fashion to the $PdCl_2$ catalyst, no products arising from either 1,2 H-addition or hydrogen addition to π-allylic structures are seen with the $Pd(NO_3)_2/Al_2O_3$ catalyst.

Following the calibration procedures described in Sec. II B and III A, and including the C-O stretch at 1050 cm^{-1} as an indicator for the presence of butan-1-ol, then enable the reaction profile for the 5 wt. % $Pd(NO_3)_2/Al_2O_3$ catalyst to be determined, Fig. 9. The profile is markedly different to that seen for the 1 wt. % $PdCl_2/Al_2O_3$ catalyst (Fig. 5). Crotonaldehyde decreases rapidly and is completely converted within ~10 min. The rate of butanal formation is rapid during this period but reaches a maximum at about 7 min. Thereafter, it progressively decreases in intensity at a much-reduced rate. Throughout this period, butan-1-ol is progressively formed. Overall, the reaction profile is entirely consistent with a consecutive reaction, where the crotonaldehyde is rapidly hydrogenated to form butanal, which is itself then more slowly hydrogenated to produce butan-1-ol. Moreover, both first stage and second stage reactions obey first order kinetics, so that the rate coefficients for each stage can be determined using classical procedures for consecutive first order reactions.[39(b)]

The concentration of crotonaldehyde at any time, t ([crotonaldehyde]$_t$) is given by the usual first order expression[39(a)]

$$[\text{crotonaldehyde}]_t = [\text{crotonaldehyde}]_0 e^{-k_1 t}, \quad (1)$$

where k_1 is the first stage rate coefficient and $[\text{crotonaldehyde}]_0$ represents the initial crotonaldehyde concentration. The expressions for butanal and butanol are given by Eqs. (2) and (3), respectively,[39(b)]

$$[\text{butanal}]_t = \frac{[\text{crontonaldehyde}]_0 k_1}{(k_2 - k_1)}(e^{-k_1 t} - e^{-k_2 t}), \quad (2)$$

$$[\text{butan} - 1 - \text{ol}]_t = [\text{crontonaldehyde}]_0 \times \left[1 + \frac{1}{(k_2 - k_1)}(k_2 e^{-k_1 t} - k_1 e^{-k_2 t})\right], \quad (3)$$

where k_2 represents the rate coefficient for the second stage hydrogenation (butanal → butanol). It is noted that Eqs. (2) and (3) represent the yield of butanal and butanol, respectively, when dividing the left-hand side of the equations by the initial crotonaldehyde concentration.

The determination of k_1 is straightforward, using the integrated rate equation for a first order reaction (Eq. (1)). The determination of k_2 uses the concentration profile of the reaction (Fig. 9), from which k_2 is obtained from a nonlinear least squares fit of the data to Eqs. (2) and (3).

The mass balance for this reaction is also presented in Fig. 9, which is determined from the sum of the absolute values of crotonaldehyde, butanal, and butanol. As with Fig. 4, a small excess is seen at short reaction times but, in marked contrast to Fig. 4, a significant mass imbalance is evident on extended reaction times. This loss is thought to represent surface chemical processes that prevent the release of material to the gas phase. Given that it is progressive and loosely scales with the butanal conversion, it is thought to represent retention or reaction of this intermediate species at the catalyst surface and thus indicates the presence of an additional and alternative pathway on this catalyst compared to that seen for the $PdCl_2$ catalyst. At 105 min, a mass balance of 69% is seen, which means that ~31% of reagents/products are not being released to the gas phase at that stage of the hydrogenation process. Decarbonylation and the formation of hydrocarbonaceous residues, as described by Englisch and co-workers for crotonaldehyde on supported Pt particles,[9] is thought to represent part of this process.

C. Kinetic analysis

The other three catalysts – 1% $Pd(NO_3)_2$, 1% Pd(acac), and 10% Pd(azide) – were examined in exactly the same fashion as described for the 1% $PdCl_2$ and 5% $Pd(NO_3)_2$ catalysts described above. All of the catalysts were active for stage 1 hydrogenation, although the rates were noticeably faster than for the 1 wt. % $PdCl_2$ sample. The 1 wt. % $PdCl_2$ catalyst was the only sample that was inactive for stage 2 hydrogenation. Contradicting Rylander's assertions,[20(a)(b)] all of the other catalysts were active for the second stage hydrogenation. That said, there was considerable variability in the rates but, nevertheless, the 1% $Pd(NO_3)_2$, 5% $Pd(NO_3)_2$, 1% Pd(acac), and 10% Pd(azide) catalysts were all able to hydrogenate the C = O functional unit to produce butanol. Rate coefficients for both first and second stage hydrogenation reactions are presented in Table I.

It is noted that it is more common in the catalytic literature to use reaction rates rather than rate coefficients to define chemical activity. This reflects the dominance of continuous-flow reactors for this type of measurement. Within the confines of the batch reactor arrangement used here, it is more appropriate to apply the relevant integrated rate expression (first order in this case) for the full data set and to use a rate coefficient to express activity. Subsequent normalisation of the rate coefficient with respect to metal surface area therefore does not equate to a conventional turnover number, for example as defined in Ref. 12(c). However, for comparative purposes, the profile presented in Fig. 5 corresponds to a turnover number of 77, i.e., the conversion of 77 crontonaldehyde molecules per surface site. Thus, the profile corresponds to many turnovers per active site, i.e., catalysis.

Given the unexpected outcome that the majority of the alumina-supported Pd catalysts were able to hydrogenate the carbonyl functionality, all of the catalysts were examined for the hydrogenation of butanal in the absence of crotonaldehyde. Following the trends outlined above, all of the catalysts with the exception of the 1 wt. % $PdCl_2$ sample were found to be active for this reaction. The associated rate coefficients are included in Table I and are identified by the descriptor k_2*.

1. First stage hydrogenation

Concentrating first on the conversion of crotonaldehyde to butanal, Fig. 10(a) shows the k_1 values for the 1% $Pd(NO_3)_2$, 5% $Pd(NO_3)_2$, 1% Pd(acac), and 10% Pd(azide) samples are similar (mean = 0.43 min^{-1}), with some significant variance between these samples and that of the catalyst derived from a $PdCl_2$ precursor (circled). A previous study using the hydrogenation of propene to estimate the relative reactivities of the 1 wt. % $Pd(NO_3)_2$, 1 wt. % $PdCl_2$, and 1 wt. % Pd(acac) catalysts showed the 1 wt. % $PdCl_2$ sample to exhibit a significantly reduced rate of reaction compared to the other two catalysts.[5] However, it is often more informative to consider the magnitude of the rate that has been normalised to the number of surface Pd atoms. This latter parameter is available from CO adsorption isotherm data.[5] The resulting k_1/Pd(s) values are tabulated in Table II and correlated against the mean Pd particle diameter in Fig. 10(b). In this manner, Fig. 10(b) then indicates how the surface normalised rate coefficient (N.B., not a turnover frequency) varies for a range of Pd catalysts whose inherent morphologies vary from extended low index planes (10% Pd(azide)) to a predominance of

TABLE I. Rate coefficient values for first (k_1) and second (k_2) stage crotonaldehyde hydrogenation reactions. The mean Pd particle diameters are derived from CO adsorption isotherm measurements (Ref. 5). k_1 is obtained from direct analysis of the crotonaldehyde conversion data and the k_2 values are obtained from modelling the crotonaldehyde reaction profile as a consecutive process exhibiting first order kinetics. k_2* represents the rate coefficient corresponding to the hydrogenation of butanal only (i.e., butanal → butanol, made in the absence of crotonaldehyde). The error values for k_1 and k_2 represent the range from a number of replicate experiments. The k_2* values are average values from duplicate measurements.

Catalyst	Mean Pd diameter (nm)	k_1 (min^{-1})	k_2 (min^{-1})	k_2* (min^{-1})
10% Pd(azide)	8.5	0.435 ± 0.045	0.027 ± 002	0.024
1% $PdCl_2$	2.5	0.277 ± 0.050	0	0
5% $Pd(NO_3)_2$	2.3	0.421 ± 0.017	0.121 ± 0.005	0.120
1% $Pd(NO_3)_2$	1.4	0.426 ± 0.064	0.020 ± 0.008	0.033
1% Pd(acac)	1.2	0.430 ± 0.009	0.010 ±0.010	0.032

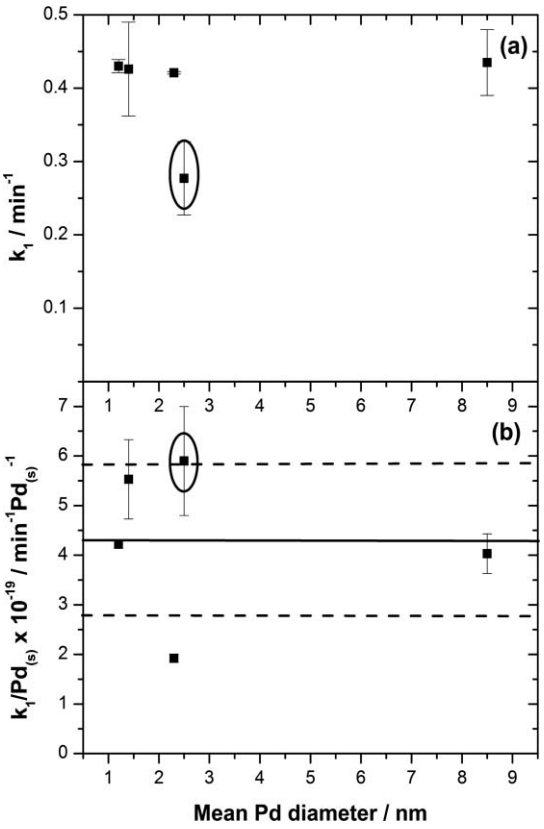

FIG. 10. (a) Plot of crotonaldehyde hydrogenation first stage rate coefficient (k_1) as a function of mean Pd particle size. (b) Plot of crotonaldehyde hydrogenation first stage rate coefficients (k_1) normalised with respect to the number of surface Pd atoms (Table II) as a function of mean Pd particle size. The solid line represents the mean value for all five samples, with the dashed lines indicating ± 1 standard deviation about the mean value. The circled data point in (a) and (b) indicates the value for the 1% $PdCl_2$ catalyst.

corner atoms (1% Pd(acac)).[5] Figure 10(b) shows a fair degree of scatter, complicating further analysis. Nevertheless, the authors' interpret this figure as indicating that all five catalysts exhibit broadly similar k_1/Pd(s) values about a mean value of 4.3×10^{-19} min^{-1} Pd(s)$^{-1}$; with the scatter defining the range about a mean value. The mean value plus 1 standard deviation represented in Fig. 10(b) by solid and dashed lines respectively seeks to illustrate this point. Assuming this interpretation to be correct, that the k_1/Pd(s) values for all five samples are effectively constant with respect to mean Pd particle size, indicates that within the 1.2 – 8.5 nm mean Pd crystallite range studied, the first stage hydrogenation reaction approximates to being *structure insensitive*.[12(a),13(a)(b)] This means that the rate of reaction, as exemplified by the rate coefficient, is effectively insensitive to the surface roughness of the Pd particles and that the rate is simply proportional to the number of surface atoms, consistent with experimental observations (Sec. II B). The fact that the smallest (1% Pd(acac)) and the largest (10% Pd(azide)) particles exhibit comparable k_1/Pd(s) values supports this assertion. With reference to numerous studies on ethene hydrogenation, this deduction is consistent with the general understanding that alkene hydrogenation reactions over supported metal catalysts are *structure insensitive*.[12(b),13(b)]

Normalisation of the experimental rate coefficient for the 1% $PdCl_2$ catalyst enhances its value relative to the other samples, indicating crotonaldehyde hydrogenation over Pd not to be poisoned by the chlorine residues present on this catalyst. Rather, it implies that the chlorine residues[5] are simply reducing the number of accessible sites. This outcome contrasts with the previous propene hydrogenation continuous-flow micro-reactor study[5] and indicates a level of variability for Pd catalysts applied to hydrogenating C = C bonds in conjugated and non-conjugated molecules.

2. Second stage hydrogenation

Table I shows reasonable agreement between the separate butanal hydrogenation experiments (k_2*) and the crotonaldehyde reactions (k_2), where the butanal reaction was seen to follow the initial crotonaldehyde conversion process. Namely, the 1% $PdCl_2$ sample that was inactive in the second stage crotonaldehyde reaction additionally exhibited no activity for butanal hydrogenation.

Figure 11(a) presents second stage crotonaldehyde rate coefficients (k_2) as a function of mean Pd diameter. Excluding the non-reactive $PdCl_2$ sample (circled), it is clear that k_2 is sensitive to particular catalyst specifications. Interestingly, it is the 5% $Pd(NO_3)_2$ catalyst, which possesses particles of intermediate dimensions,[5] that exhibits the highest k_2 value. Following the approach adopted in Sec. III C 1, the k_2 values normalised with respect to surface Pd atoms are presented in Table II and Fig. 11(b), with the latter indicating a distinctly non-linear dependence with respect to particle size. The trend for the k_2/Pd(s) values is described below:

$$5\%\,Pd(NO_3)_2 > 1\%\,Pd(NO_3)_2 > 10\%\,Pd(azide)$$
$$> 1\%\,Pd(acac) \gg 1\,wt\%\,PdCl_2.$$

A line is presented in Fig. 11(b) that is intended to define the generalised trend. The 1 wt. % $PdCl_2$ catalyst (circled)

TABLE II. Rate coefficient values for first (k_1) and second (k_2) stage crotonaldehyde hydrogenation reactions (Table I) normalised with respect to the number of Pd surface atoms. The last column presents the Pd surface normalised rate coefficient measured for the butanal hydrogenation reaction (Table I).

Catalyst	Mean Pd diameter (nm)	$k_1/Pd_{(s)}$ (min^{-1} $Pd_{(s)}^{-1}$)	$k_2/Pd_{(s)}$ (min^{-1} $Pd_{(s)}^{-1}$)	k_2*/$Pd_{(s)}$ (min^{-1} $Pd_{(s)}^{-1}$)
10% Pd(azide)	8.5	$4.03 \pm 0.4 \times 10^{-19}$	$2.50 \pm 0.2 \times 10^{-20}$	2.2×10^{-20}
1% $PdCl_2$	2.5	$5.90 \pm 1.1 \times 10^{-19}$	0	0
5% $Pd(NO_3)_2$	2.3	$1.92 \pm 0.1 \times 10^{-19}$	$5.48 \pm 0.2 \times 10^{-20}$	5.5×10^{-20}
1% $Pd(NO_3)_2$	1.4	$5.53 \pm 0.8 \times 10^{-19}$	$4.28 \pm 1.7 \times 10^{-20}$	4.3×10^{-20}
1% Pd(acac)	1.2	$4.22 \pm 0.1 \times 10^{-19}$	$0.98 \pm 1.1 \times 10^{-20}$	3.1×10^{-20}

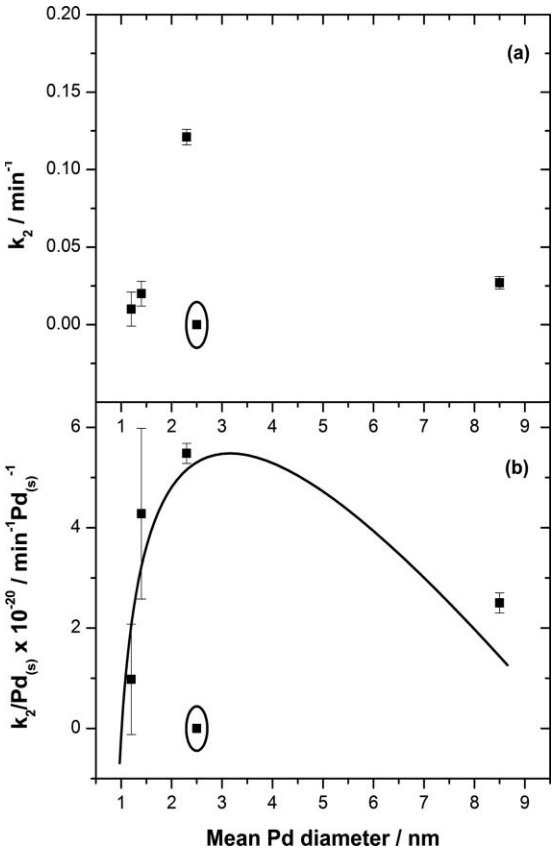

FIG. 11. (a) Plot of crotonaldehyde hydrogenation second stage rate coefficient (k_2) as a function of mean Pd particle size. (b) Plot of crotonaldehyde hydrogenation second stage rate coefficients (k_2) normalised with respect to the number of surface Pd atoms as a function of mean Pd particle size. The solid line in (b) is presented as a guide to the eye and is intended to indicate correlation between the data points with the exception of the 1% $PdCl_2$ catalyst, which is inactive for this reaction. The circled data point in (a) and (b) indicates the value for the 1% $PdCl_2$ catalyst.

has been excluded from the trend-line, as it is inactive for this stage of the reaction process (Table I and Sec. III A).

Similar plots linking catalytic activity and particle size have been reported previously. Notably, Murzin, and Simakova [41] have analysed ethene hydrogenation data over supported palladium catalysts originally reported by Binder and co-workers [42] and have shown a marked particle size dependency. Murzin's model takes a thermodynamic approach that accounts for the chemical potential on adsorption as a function of metal particle size. More recently, Sotoodeh and Smith have also observed similar trends for a structure sensitivity of dodecahydro-N-ethylcarbazole dehydrogenation over Pd catalysts.[43] So, given that the trend established in Fig. 11(b) is not unprecedented, what are its origins in the case of crotonaldehyde hydrogenation over alumina-supported Pd catalysts?

First, on initial inspection, the non-linearity of the curve in Fig. 11(b) indicates the stage 2 hydrogenation to be *structure sensitive.*[12(a)] This is in direct contrast to that seen for the first hydrogenation step (Sec. III C 1). Thus, the butanal → butanol reaction appears to be sensitive to the morphology of the Pd particles. Previous work using infrared spectroscopy has deduced the nature of the Pd sites that each of the five catalysts present.[5] The large Pd (azide) particles (8.5 nm diameter) are strongly dominated by low index planes, although inevitably there are also a small number of edge sites. At the other end of the scale the small Pd(acac) particles (1.2 nm diameter) are dominated by corner atoms, having insufficient atoms to define a particular surface plane. Yet, as both of these samples exhibit relatively low hydrogenation activities, neither of these attributes can be individually responsible for favourable turnover. Given that maximum activity more closely correlates with the 1% and 5% $Pd(NO_3)_2$ samples (Table II, Fig. 11(b)), the source for the enhanced activity for this process is thought to be edge atoms. More specifically, following previous vibrational assignments that were able to distinguish corner and edge adsorption sites for this suite of Pd catalysts,[5] (111)/(111) and (111)/(100) particle edges are implicated as being responsible for the second stage activity. In this manner, the Pd(acac) particles, which only convey corner sites, have negligible activity, whereas the low activity of the Pd (azide) particles arises from the relatively low concentration of edge sites on these particles. Transmission electron microscopy shows the shape of these larger particles of the Pd(azide) sample to approximate to cubo-octahedra,[8] which will feature extended (111) and (100) planes. The relatively reduced activity seen for this catalyst is therefore attributed to the relatively small number of atoms present at the interface between these planes.

From inspection of the CO stretching frequencies, only the 1 wt. % $PdCl_2$ sample was thought to be contaminated by surface residues.[5] This therefore eliminates the possibility that the favourable performance of the 1% and 5% $Pd(NO_3)_2$ catalysts, as evidenced in Fig. 11(b), is attributable either to the presence or the absence of a surface residue. Rather, focussing on particle morphology, the heightened hydrogenation activity for these samples can be correlated with their particle size being able to support a maximum density of edge sites. An increase in size beyond ~2.5 nm will lead to a reduction in the absolute number of these sites, as described in the pioneering work of van Hardeveld and Hartog.[44] The situation for particles smaller than ~1.4 nm is more intricate. Crucially, it relates to distinguishing between corner and edge sites. For the purposes of this discussion, an edge site is defined as a distinct junction between two specific surface planes, in this case the (111)/(111) and (111)/(100) planes. Crystallographic considerations establish that the edge between (111) and (111) planes is a (110) microfacet, whereas the edge between the (111) and (100) planes is a (331) microfacet. Further, the angle between the (111) and (100) planes is 54.7°.[45] The electronic configuration for these edge atoms is distinct and reflects the local bonding geometry of that site. Corner atoms could be at the extreme ends of these edge sites but, more pertinently, we consider these atoms to also be at the surface of very small particles where there is insufficient atom density to define surface planes. Thus, for very small particles, the surface atoms tend to be dominated by corner atoms. Temperature programmed infrared spectroscopy (TP-IRS) performed under pulse-flow conditions and using CO as a probe molecule is able to differentiate between corner and edge Pd atoms.[5] For example, linear CO on the Pd(acac) catalyst exhibits a single intense feature at 2077 cm^{-1} that is

assigned to corner atoms. However, the 5% $Pd(NO_3)_2$ catalyst displays two features: a peak at 2079 cm^{-1} due to corner sites but also a peak at 2050 cm^{-1}, which is assigned to linear CO residing on (111)/(111) and (111)/(100) edges. If corner atoms were relevant to the stage 2 hydrogenation process, then the Pd(acac) catalyst would be expected to have the highest k_2 value. Instead, as Table II and Fig. 11 show, this sample actually has the lowest value of the four catalysts that are active for this reaction. It is assumed that the relative inactivity of these corner atoms is an electronic effect, where their local electronic structure is somehow constraining their hydrogenation activity. Possibly linked to this deduction, it is noted that TP-IRS reveals the enthalpy of CO adsorption on these sites to be lower than that for the equivalent state on the edge sites.[5]

The 1% $Pd(NO_3)_2$ catalyst possesses both corner and edge sites and its lower k_2/Pd(s) value compared to its higher metal loading counterpart is readily attributed to the latter presenting a higher concentration of edge sites. The situation pertaining to the 10% Pd(azide) catalyst requires careful inspection of its chemisorbed CO infrared spectrum, which is dominated by bridge bonded CO peaks at 1984 and 1923 cm^{-1}.[5] However at saturation CO exposures, two weak features are discernible at 2081 and 2064 cm^{-1}, which can be assigned to corner and edge atoms respectively. Contrasting the particle morphology for this catalyst with respect to the Pd(acac) sample indicates that it is the edge atoms that are primarily responsible for the observed k_2/Pd(s) value. Importantly, the outcome for the Pd(azide) catalyst also indicates that low index planes have negligible stage 2 activity. Thus, the picture that is emerging is one where stage 1 activity is *structure insensitive* and that activity can be broadly correlated with the number of surface Pd atoms, with no preference apparent for particular morphological traits of the Pd crystallites. Similar trends have been reported previously for ethene hydrogenation[46,47] and butadiene hydrogenation[48] over Pd-alumina model catalysts.

On the other hand, stage 2 is *structure sensitive*, where hydrogenation activity can be specifically correlated with the presence of (111)/(111) and (111)/(100) edges of the Pd crystallites. The greater the concentration of these edge sites, the higher the hydrogenation rate. Low index planes, e.g., (111) and (100), are not effective in stage 2 chemistry. However, although this description invokes a primarily geometric perspective, it additionally acknowledges that corner sites could be attenuated via an electronic component that is a reflection of their specific bonding arrangements.

The above analysis seeks to rationalise the trends displayed in Fig. 11 for the 1% Pd(acac), 1% $Pd(NO_3)_2$, 5% $Pd(NO_3)_2$ and 10% Pd(azide) catalysts. The next question to answer is how does the 1 wt. % $PdCl_2$ catalyst operate with respect to hydrogenation of the saturated aldehyde? Interestingly, this catalyst displays good activity for the hydrogenation of the unsaturated aldehyde (Fig. 10). Thus, it seems unlikely that a constrained hydrogen supply, invoked as a possible reason for the diminished rate in continuous flow propene hydrogenation experiments,[5] is the issue in these batch reactor experiments. So, if it is not the hydrogen, one is forced to invoke constraints to the adsorption of the butanal. This links in with this catalyst uniquely containing chemical residues (5.4 wt. % Cl, see Introduction section). Whereas the majority of the chlorine will be associated with the alumina,[49] a proportion will additionally be bound to the metal. Now, infrared spectroscopy provides evidence that this chlorine is present within the Pd low index planes and, most crucially, at the Pd particle edges.[5] In this manner, it is assumed that although the Pd particles of mean diameter 2.5 nm are ideally set up with edge sites that convey stage 2 hydrogenation activity, it transpires that these sites are chemically poisoned by the chlorine, which then makes this catalyst inactive for butanal hydrogenation.

Concentrating specifically on the role of crystallite morphology, Fig. 12 schematically illustrates the two modes in which the Pd catalysts operate with respect to crotonaldehyde hydrogenation reactions. It is acknowledged that turnover is unlikely to take place on pristine metal surfaces, more likely hydrocarbonaceous overlayers will be present as part of the catalyst conditioning process[50–52] but, nevertheless, given that the precise nature of the overlayers are unknown at this time, such features are not considered within Fig. 12. Rather, the figure seeks to state the metal crystallite morphology that ultimately defines the actual active sites.

First, it is assumed that hydrogenation of the crotonaldehyde can occur on a wide variety of Pd sites. Figure 12(a) illustrates the mode of action, illustrating the case how the C = C double bond can bind to a low index plane. A di-σ interaction is assumed,[24] although the specifics of that interaction are beyond the scope of these investigations. Figure 12(b) illustrates the case for butanal hydrogenation. Here it is postulated that the carbonyl binds in a di-σ configuration in a manner that requires the presence of an edge site. Specifically, it is thought that the edge site is required to coordinate with the lone pair of electrons on the oxygen. This proposition, if correct, could be the origin for the selectivity to butanol. For complete conversion of crotonaldehyde to butanol both sites, as illustrated in Fig. 12, need to be present on the Pd crystallites.

It is informative to speculate how these collective observations could be rationalised within the assertion by Rylander that, except under vigorous conditions,[40] reduction of α,β-unsaturated aldehydes by supported palladium catalysts will be highly selective to the saturated aldehyde, with the Pd being inactive for the reduction of the aliphatic carbonyl.[20(a)] One possibility could be that Rylander's catalysts were not as well dispersed as the materials studied here. Making the comparison to Table I and Fig. 11(a) it is apparent that the observed hydrogenation rate for stage 2 is highly dependent on particle size and a significant decrease in rate is anticipated for particles of diameter greater than 10 nm.

This study indicates that there are at least two practical control parameters that a catalytic chemist could use to modify reaction profiles for the hydrogenation of α,β-unsaturated aldehydes, and also possibly other molecular entities, over high surface area Pd catalysts. First, high selectivity to the saturated aldehyde can be achieved by application of large Pd particles. Their relatively low density of edge sites [44] will ensure a low rate for butanal hydrogenation. However, particularly given current market values for Pd, this is an inefficient

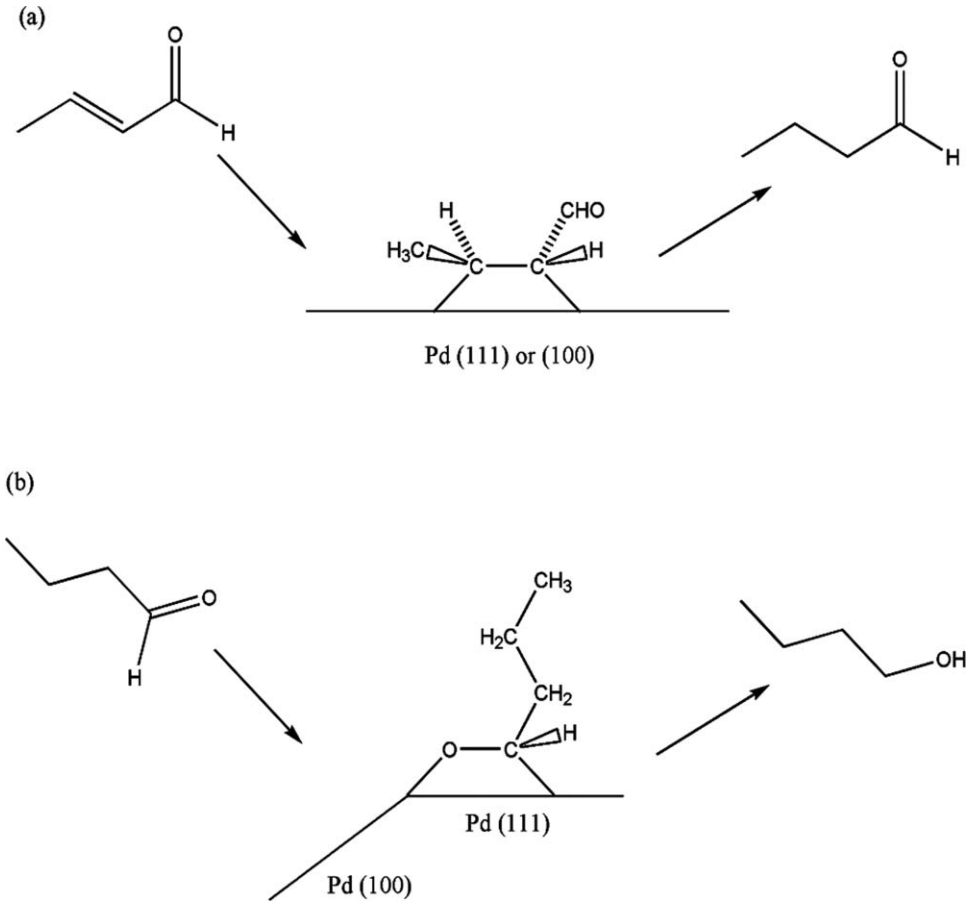

FIG. 12. Schematic representation for (a) the first and (b) second stages of the crotonaldehyde hydrogenation process. The reduction of cotonaldehyde to produce butanal can occur at any Pd site. The reduction of butanal to produce butanol is supported by the presence/availability of (111)/(111) and (111)/(100) edge sites that are believed to facilitate the hydrogenation process. Both sites (a) and (b) are thought to involve the presence of a hydrocarbonaceous overlayer which forms as part of the initial catalyst conditioning process (see text). That overlayer is not represented in this diagram. The precise adsorption geometries for the crotonaldehyde and the butanal molecules are unknown at present.

and expensive route, making poor use of the valuable precious metal. A more cost effective route would be to selectively poison edge sites, so the second stage hydrogenation is forbidden. Presumably a number of poisons could be considered. However, this work shows that a poisoning strategy could be incorporated in to the catalyst preparative procedures by using salts and auxiliary compounds (dilute HCl was used as a solvent in the preparation of the $PdCl_2$ catalyst [5]) for which preparative procedures inherently leave residues present at the catalyst surface. In the case examined here, it is suggested that these residues effectively "cap" edge sites, making the catalyst unable to hydrogenate butanal and maintaining high selectivity for the saturated aldehyde. In the modest pressure and batch conditions used here, the $PdCl_2$ sample was 100% selective to butanal.

3. Butanal hydrogenation and chemisorption

In order to confirm the validity and relevance of the outcome that four of the five catalysts studied here exhibited poor selectivity to the saturated alcohol if the hydrogen consumption was allowed to proceed beyond 100% conversion (i.e., complete conversion of crotonaldehyde), the hydrogenation of butanal was additionally examined. Table I and Fig. 13(a) show that the general trends seen for crotonaldehyde stage 2 performance are essentially reproduced for the direct butanal hydrogenation reaction, k_2*. Most notably, only the $PdCl_2$ sample was inactive for this reaction. The magnitude of the rate coefficient for the isolated reaction (k_2*) compares most favourably with k_2 values for the 5% $Pd(NO_3)_2$ and 10% Pd(azide) samples but the former is noticeably greater for the 1% $Pd(NO_3)_2$ and 1% Pd(acac) samples (Table I). Given the variability that pre-adsorption and reaction of crotonaldehyde could make regards potentially modifying the Pd surface, *e.g.* by modification of the carbon laydown process as signified by the mass imbalance indicated in Fig. 9, this is not a totally unsurprising outcome. Nevertheless, the fact that the profile of Fig. 13(a) very closely matches that of Fig. 11(a) is taken as strong evidence for the validity of statements made in Sec. III C 2 and reflects genuine selectivity constraints for these substrates.

The k_2*/Pd(s) values are presented in Table II and Fig. 13(b) presents the correlation with respect to Pd particle size. Essentially Fig. 13(b) replicates Fig. 11(b), confirming the *structure sensitive* nature of this reaction over these supported Pd catalysts.

It was asserted in Sec. III C 2 that a key part of the surface chemistry that effectively controls the selectivity

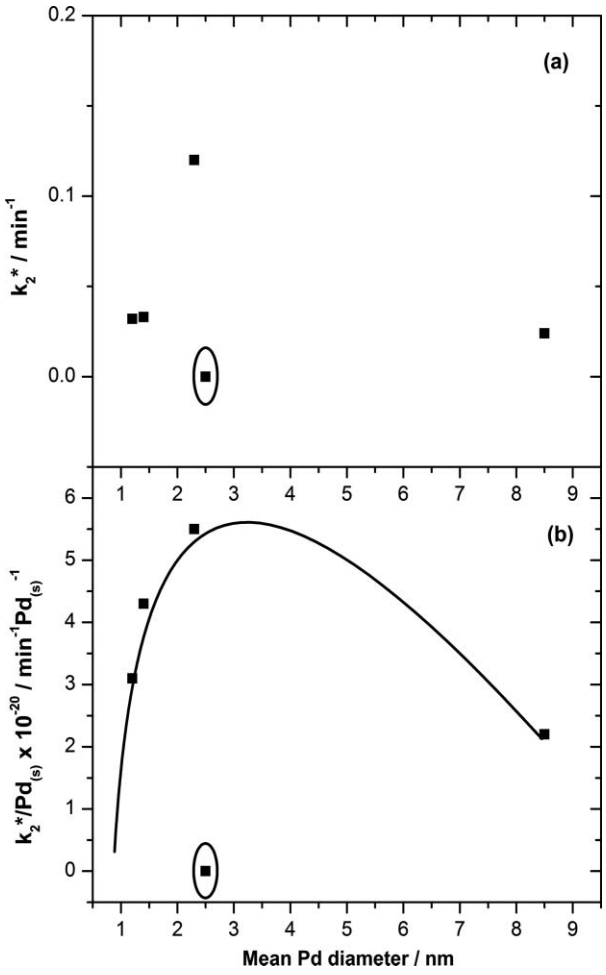

FIG. 13. (a) Plot of butanal rate coefficient (k_2*) as a function of mean Pd particle size for the five catalysts studied. (b) Plot of butanal rate coefficient (k_2*) normalised with respect to the number of surface Pd atoms as a function of mean Pd particle size. The solid line in (b) is presented as a guide to the eye and is intended to indicate correlation between the data points with the exception of the 1% $PdCl_2$ catalyst, which is inactive for this reaction. The circled data point in (a) and (b) indicates the value for the 1% $PdCl_2$ catalyst.

characteristics for the crotonaldehyde hydrogenation process over supported Pd catalysts must be the adsorption of butanal. In order to evaluate this parameter further, infrared spectroscopy was applied to investigate the adsorption of butanal over all five catalysts following the normal reduction procedure. These measurements were performed using a pulse-flow methodology, with the sample contained within a diffuse reflectance environmental cell. Thus, these measurements include a contribution from the catalyst that was absent from the simpler gas phase measurements presented in Secs. III A and III B. Blank adsorption experiments (not shown) on plain alumina produced minor changes in the infrared spectrum. Namely, a small loss of isolated hydroxyl groups (~3700 cm^{-1}) and a small loss of water, as signified by a negative feature about 1620 cm^{-1} (δ(O-H) H_2O). However, no butanal features were observable, indicating the support to play a negligible role in the adsorption process. Figure 14 presents representative spectra for butanal exposed to the 1% Pd(acac) and 1% $PdCl_2$ catalysts.

Figure 14(a) presents the spectrum for the 1% Pd(acac) catalyst. Bands exhibiting a negative inflection are seen at

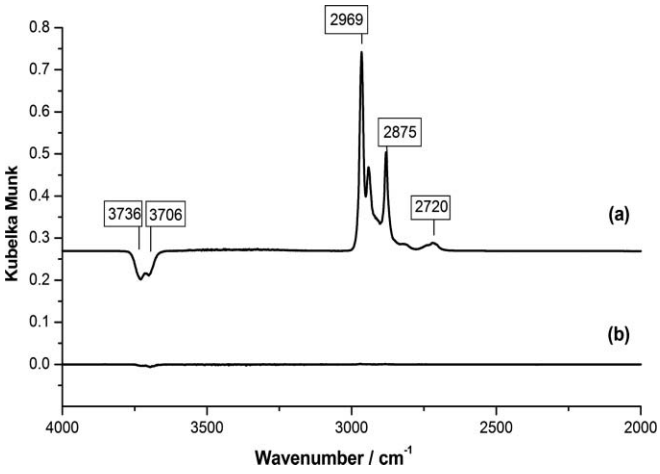

FIG. 14. Diffuse reflectance infrared spectra for butanal exposed to (a) 1% Pd(acac) and (b) 1% $PdCl_2$ at 293 K using a pulse-flow arrangement. The catalysts were reduced prior to butanal exposure. The spectra represent difference spectra, where a spectrum from the reduced catalyst has been subtracted for the spectrum of the catalyst after exposure to butanal.

3736 and 3706 cm^{-1}. These are assigned to the (O-H) stretching modes of terminal hydroxyl groups present on the alumina support material.[35] The negative inflection indicates that there is some adsorption on the support material as well as on the metal. The intensity of these features substantially exceeds that seen for the alumina blank (not shown), suggesting that this action is in fact metal-mediated and possibly represents a degree of spillover.[6] Bands in the (C-H) stretching region are seen at 2969, 2938, and 2875 cm^{-1}, that are assigned to aliphatic ν(C-H) modes of chemisorbed butanal. A weak feature is seen on the tail of the 2875 cm^{-1} peak that is centred at 2811 cm^{-1} and a stronger band is seen at 2720 cm^{-1}. These are assigned to aldehyde C-H bands [ν(C-H) and 2 $\times$ ρ(C-H), respectively] signifying the presence of the aldehyde functional unit.[36(a)] Relative to the aliphatic ν(C-H) modes of butanal in the gas phase,[37(b)] the aldehyde modes in Fig. 14(a) are significantly attenuated, consistent with adsorption to the metal occurring via this functional unit. Comparable measurements on the 1% $Pd(NO_3)_2$, 5% $Pd(NO_3)_2$, and 10% Pd(azide) catalysts (not shown) established butanal to similarly chemisorb on all of these surfaces. It is noted that significant differences in the spectra corresponding to butanal adsorption on the four aforementioned catalysts were observed. These events are consistent with the mass imbalance seen in Fig. 9 for the 5% $Pd(NO_3)_2$ catalyst (Sec. III C 2) and indicate a degree of dissociative adsorption in the absence of an overpressure of hydrogen for some of the samples to be evident. It is acknowledged that further work is required to elucidate the precise nature of the chemisorbed state of butanal in the presence and absence of hydrogen. That important topic is deemed to be beyond the remit of the current study.

Figure 14(b) presents the spectrum for the 1% $PdCl_2$ catalyst. It contrasts dramatically with the spectrum for the Pd(acac) sample (Fig. 14(a)) in that it shows no signal in the ν(C-H) region of the spectrum, indicating no molecular adsorption on this surface. Despite the absence of hydrocarbon modes, very weak negative inflections at 3732 and 3698 cm^{-1} are seen, which similarly can be attributed to loss of

terminal hydroxyl groups. The reduced intensity of the hydroxyl groups in Fig. 14(b) compared 14(a) is consistent with no chemisorption involving the metal and hence no spillover of material on to the support. The connection between butanal adsorption and support hydroxyl groups remains uncertain at present but, nevertheless, it is clearly apparent from inspection of Fig. 14 that butanal adsorbs on the Pd(acac) sample but that no adsorption is apparent on the $PdCl_2$ sample. This observation is entirely consistent with the concept that the edge sites, which are required for butanal adsorption, are blocked by residual chlorine atoms (see Sec. III C 2).

Finally, this work has established a structure/activity correlation for supported Pd catalysts applied to the hydrogenation of an α,β-unsaturated aldehyde. It is possible that this reaction could be used to screen or characterise other supported palladium catalysts as an indication of their particle morphology. Moreover, it is interesting to speculate whether the concepts formulated here are applicable to other α,β-unsaturated carbonyls. Work is currently underway in our laboratories to investigate this latter enticing possibility.

IV. CONCLUSIONS

Five alumina-supported palladium catalysts, previously characterised by a combination of CO chemisorption and infrared spectroscopy, have been examined using the hydrogenation of crotonaldehyde as a test reaction. These studies establish a role for metal crystallite morphology in influencing catalyst performance. The main results can be summarised as follows:

- Using a modified infrared gas cell as a batch reactor, periodic scanning of the infrared spectrum of the gaseous phase present over the Pd/Al_2O_3 catalysts successfully generated reaction profiles.
- Four of the catalysts were able to facilitate a 2-stage hydrogenation process (crotonaldehyde → butanal → butanol), whilst one catalyst (1% $PdCl_2$) was totally selective for the first stage hydrogenation process (crotonaldehyde → butanal).
- Rate coefficients were obtained for the first and second stage hydrogenation reactions. For the first stage process, normalising rate coefficients with respect to the number of surface Pd atoms indicated the reaction to be *structure insensitive* where, within the particle size range studied, first stage hydrogenation activity is effectively independent of particle morphology.
- The second stage rate coefficients showed a marked dependency on particle size. Normalising the rate coefficients with respect to Pd surface atoms confirmed this reaction to be *structure sensitive*. Correlating the magnitude of the normalised rate coefficients with Pd particle morphology identified edge sites as being at least partially responsible for the hydrogenation of butanal to butanol.
- The $PdCl_2$ catalyst displayed a nearly complete mass balance during the course of the reaction, suggesting deactivation pathways not to predominate on this sample under these conditions. However, a mass imbalance of 31% was seen at 105 min for the 5% $Pd(NO_3)_2$ sample, which is linked to the dissociative adsorption of butanal.
- The inactivity of the 1% $PdCl_2$ catalyst for the second stage hydrogenation process was attributed to the edge sites of these Pd particles being poisoned by chlorine atoms that originate from the catalyst preparative process.
- Infrared measurements of butanal adsorption on all five catalysts showed adsorption failed to occur only on the 1% $PdCl_2$ catalyst. Thus, the inability of this sample to adsorb the product from the first stage hydrogenation process is linked to the 100% selectivity to butanal seen for the crotonaldehyde hydrogenation measurements over this catalyst.

ACKNOWLEDGMENTS

Financial assistance from the ICI Strategic Research Fund is gratefully acknowledged (D.L.) The University of Glasgow and ICI are thanked for the provision of a Ph.D. studentship (T.L.) The Erasmus Scheme of the EU Lifelong Learning Programme is thanked for student support (A.U.) The Scottish Higher Education Funding Council is thanked for the provision of a Research Development Grant (D.L.)

[1] D. L. Trimm, *Design of Industrial Catalysts* (Elsevier, Amsterdam, 1980).
[2] G. A. Somorjai and J. Y. Park, J. Chem. Phys. **128**, 182504 (2008).
[3] I. Lee, F. Delbecq, R. Morales, M. A. Albiter, and F. Zaera, Nature Mater. **8**, 134 (2009).
[4] A. M. Molenbroek, S. Helvig, H. Topsøe, and B. S. Clausen, Top. Catal. **52**, 1303 (2009).
[5] T. Lear, R. Marshall, J. A. Lopez-Sanchez, S. D. Jackson, T. M. Klapötke, M. Bäumer, G. Rupprechter, H-J. Freund, and D. Lennon, J. Chem. Phys. **123**, 174706 (2005).
[6] D. R. Kennedy, G. Webb, S. D. Jackson, and D. Lennon, Appl. Catal., A **259**, 109 (2004).
[7] R. Marshall, G. Webb, S. D. Jackson, and D. Lennon, J. Mol. Catal. A: Chem. **226** 227 (2005).
[8] T. Lear, R. Marshall, E. K. Gibson, T. Schütt, T. M. Klapötke, G. Rupprechter, H-J. Freund, J. M. Winfield, and D. Lennon, Phys. Chem. Chem. Phys. **7**, 565 (2005).
[9] M. Englisch, A. Jentys, and J. A. Lercher, J. Catal. **166**, 25 (1997).
[10] P. Claus, Top. Catal. **5**, 51 (1998).
[11] P. Claus and H. Hofmeister, J. Phys. Chem. B **103**, 2766 (1999).
[12] G. A. Somorjai, *Introduction to Surface Chemistry and Catalysis* (Wiley, New York, 1994), (a) p. 453; (b) p. 509; (c) p. 446.
[13] G. C. Bond, *Metal-Catalysed Reactions of Hydrocarbons* (Springer, New York, 2005), (a) p. 231; (b) p. 303; (c) p. 231; (d) 304; (e) p. 232.
[14] E. Gebauer-Henke, J. Grams, E. Szubiakiewicz, J. Farbotko, R. Touroude, and J. Rynkowski, J. Catal. **250**, 195 (2007).
[15] J. E. Baile, and G. J. Hutchings, Chem. Commun. 2151 (1999).
[16] R. Zanella, C. Louis, S. Giorgio, and R. Touroude, J. Catal. **223**, 328 (2004).
[17] E. V. Ramos-Fernández, B. Samaranch, P. Ramírez de la Piscina, N. Homs, J. L. G. Fierro, F. Rodríguez-Reinoso, and A. Sepúlveda-Escribano, Appl. Catal., A **349**, 165 (2008).
[18] D. Divakar, D. Manikandan, V. Rupa, E. L. Preethi, R. Chandrasekar, and T. Sivakumar, J. Chem. Technol. Biotechnol. **82**, 253 (2007).
[19] T. Seki, J-D. Grunwaldt, N. van Vegeten, and A. Baiker, Adv. Synth. Catal. **350**, 691 (2008).
[20] P. N. Rylander, *Catalytic Hydrogenation over Platinum Metals* (Academic, New York, 1967), (a) p. 107; (b) p. 250.
[21] J. C. de Jesús and F. Zaera, Surf. Sci. **430**, 99 (1999).
[22] E. Janin, H. Schenck, S. Ringler, J. Weissenrieder, T. Åkermark, and M. Göthelid, J. Catal. **215**, 245 (2003).
[23] D. I. Jerdev, A. Olivas, and B. E. Koel, J. Catal. **205**, 278 (2002).

[24]J. Haubrich, D. Loffreda, F. Delbecq, P. Sautet, A. Krupski, C. Becker, and K. Wandelt, J. Phys. Chem. C **113**, 13947 (2009).
[25]A. J. Urquhart, F. J. Williams, O. P. H. Vaughan, R. L. Cropley, and R. M. Lambert, Chem. Comm. 1977 (2005).
[26]M. E. Chiu, G. Kyriakou, F. J. Williams, D. J. Watson, M. S. Tikhov, and R. M. Lambert, Chem. Comm. 1283 (2006).
[27]G. J. Hutchings, F. King, I. P. Okoye, M. B. Padley, and C. H. Rochester, J. Catal. **148**, 453 (1994).
[28]G. J. Hutchings, F. King, I. P. Okoye, M. B. Padley, and C. H. Rochester, J. Catal. **148**, 464 (1994).
[29]C. J. Kliewer, M. Bieri, and G. A. Somorjai, J. Am. Chem. Soc. **131**, 9958 (2009).
[30]S. D. Jackson, S. Munro, P. Colman and D. Lennon, Langmuir **16**, 6519 (2000).
[31]E. Opara, D. T. Lundie, T. Lear, I. W. Sutherland, S. F. Parker, and D. Lennon, Phys. Chem. Chem. Phys. **6**, 5588 (2004).
[32]A. McFarlane, L. McMillan, I. Silverwood, N. G. Hamilton, D. Siegel, S. F. Parker, D. T. Lundie, and D. Lennon, Catal. Today **155**, 206 (2010).
[33]D. Siegel, N. G. Hamilton, J. Kapitan, L. Hecht, D. Lennon, and S. F. Parker (unpublished).
[34]T. Lear, N. G. Hamilton, and D. Lennon, Catal. Today **126**, 219 (2007).
[35]D. T. Lundie, A. R. McInroy, R. Marshall, J. M. Winfield, P. Jones, C. C. Dudman, S. F. Parker, C. Mitchell, and D. Lennon, J. Phys. Chem. B **109**, 11592 (2005).
[36]D. Lin-Vien, N. B. Colthup, W. G. Fateley, and J. G. Grasselli, *The handbook of Infrared and Raman Characteristic Frequencies of Organic Molecules* (Academic, New York, 1991), (a) p. 122; (b) p. 89; (c) p. 124; (d) p. 57; (e) p. 46.
[37]C. J. Pouchert, *The Aldrich Library of FT-IR Spectra*, 1st Ed. (Aldrich Chemical Company, Milwaukee, 1985), Vol. 1, (a) p. 466; (b) p. 138.
[38]J. R. Durig, S. C. Brown, V. F. Kalasinsky, and W. O. George, Spectrochim. Acta **32A**, 807 (1976).
[39]B. G. Cox, *Modern Liquid Phase Kinetics* (Oxford University Press, Oxford, 1996), (a) p. 7; (b) p. 28.
[40]P. N. Rylander and N. Himelstein, Engelhard Ind. Tech. Bull. **4**, 131 (1964).
[41]D. Y. Murzin and I. L. Simakova, Kinet. Catal. **51**, 828 (2010).
[42]A. Binder, M. Seipenbusch, M. Muhler, and G. Kasper, J. Catal. **268**, 150 (2009).
[43]F. Sotoodeh and K. Smith, J. Catal. **279**, 36 (2011).
[44]R. van Hardeveld and F. Hartog, Adv. Catal. **22**, 75 (1972).
[45]G. Rupprechter, Phys. Chem. Chem. Phys. **3**, 4621 (2001).
[46]Sh. Shaikhutdinov, M. Heemeier, M. Bäumer, T. Lear, D. Lennon, R. J. Oldman, S. D. Jackson, and H.-J. Freund, J. Catal. **200**, 330 (2001).
[47]H-J. Freund, M. Bäumer, J. Libuda, T. Risse, G. Rupprechter, and S. Shaikhutdinov, J. Catal. **216**, 223 (2003).
[48]J. Silvestre-Albero, G. Rupprechter and H.-J. Freund, Chem. Commun. 80 (2006).
[49]A. R. McInroy, D. T. Lundie, J. M. Winfield, C. C. Dudman, P. Jones, S. F. Parker, and D. Lennon, Catal. Today **114**, 403 (2006).
[50]G. Webb, Catal. Today **7**, 139 (1990).
[51]B. Brandt, J-H Fischer, W. Ludwig, J. Libuda, F. Zaera, S. Schauermann, and H-J. Freund, J. Phys. Chem. C **112**, 11408 (2008).
[52]M. Wilde, K. Fukutani, W. Ludwig, B. Brandt, J-H Fischer, S. Schauermann, and H-J. Freund, Angew. Chem., Int. Ed. **47**, 9289 (2008).